

Observation of resonances in the reaction $\bar{p}p \rightarrow \pi^0\eta\eta$ at 1.94 GeV/c

The CRYSTAL BARREL Collaboration

A. Abele⁸, B. Adomeit⁷, C. Amsler¹⁵, C.A. Baker⁵, B.M. Barnett³, C.J. Batty⁵, M. Benayoun¹², A. Berdoz¹³, K. Beuchert², S. Bischoff⁸, P. Blüm⁸, K. Braune¹¹, D.V. Bugg⁹, T. Case¹, O. Cramer¹¹, V. Credé³, K.M. Crowe¹, T. Degener², N. Djaoshvili⁸, S. von Dombrowski^{15, 16}, M. Doser⁵, W. Dünnweber¹¹, A. Ehmanns³, D. Engelhardt⁸, M.A. Faessler¹¹, P. Giaritta¹⁵, R.P. Haddock¹⁰, F.H. Heinsius^{1, 16}, M. Heinzelmann¹⁵, A. Herbstrith⁸, M. Herz³, N.P. Hessey¹¹, P. Hidas⁴, C. Hodd⁹, C. Holtzhausen⁸, D. Jannik^{11, 16}, H. Kalinowsky³, B. Kämmler⁷, P. Kammel¹, J. Kisiel^{9, 16}, E. Klempt³, H. Koch², M. Kunze², U. Kurilla², M. Lakata¹, R. Landua⁹, J. Lüdemann^{2, 16, 17}, H. Matthäy², R. McCrady¹³, J. Meier⁷, C.A. Meyer¹³, L. Montanet⁹, R. Ouared⁹, F. Ould-Saada¹⁵, K. Peters², B. Pick³, C. Pietra¹⁵, C.N. Pinder⁵, M. Ratajczak², C. Regenfus¹¹, S. Resag³, W. Röthel¹¹, P. Schmidt⁷, R. Seibert⁷, S. Spanier¹⁵, H. Stöck^{2, 18}, C. Straßburger³, U. Strohbusch⁷, M. Suffert¹⁴, J.S. Suh³, U. Thoma³, M. Tischhäuser⁸, I. Uman¹¹, C. Völcker¹¹, S. Wallis¹¹, D. Walther^{3, 16}, U. Wiedner⁹, K. Wittmack³, and B. Zou⁹

¹ University of California, LBL, Berkeley, CA 94720, USA

² Universität Bochum, D-44788 Bochum, FRG

³ Universität Bonn, D-53115 Bonn, FRG

⁴ Academy of Science, H-1525 Budapest, Hungary

⁵ Rutherford Appleton Laboratory, Chilton, Didcot OX11 0QX, UK

⁶ CERN, CH-1211 Genève, Switzerland

⁷ Universität Hamburg, D-22761 Hamburg, FRG

⁸ Universität Karlsruhe, D-76021 Karlsruhe, FRG

⁹ Queen Mary and Westfield College, London E1 4NS, UK

¹⁰ University of California, Los Angeles, CA 90024, USA

¹¹ Universität München, D-85748 München, FRG

¹² LPNHE Paris VI, VII, F-75252 Paris, France

¹³ Carnegie Mellon University, Pittsburgh, PA 15213, USA

¹⁴ Centre de Recherches Nucléaires, F-67037 Strasbourg, France

¹⁵ Universität Zürich, CH-8057 Zürich, Switzerland

Received July 13, 1998

Abstract. Antiproton-proton annihilation into $\pi^0\eta\eta$ has been studied with the Crystal Barrel spectrometer at CERN at an incident beam momentum of 1.94 GeV/c. The data were taken with a trigger requiring neutral final states. A new isovector state, the $a_2(1660)$ decaying to $\pi^0\eta$, is observed. In the $\eta\eta$ invariant mass region around 2.1 GeV/c², strong production of a heavy resonance is required, but our analysis does not distinguish between $J^P = 0^+, 2^+$ and 4^+ . The production of the $f_0(1500)$ in reactions in flight is also observed.

1 Introduction

This is the first of several papers which will concern $\bar{p}p \rightarrow 3\pi^0$, $2\pi^0\eta$, $\pi^0\eta\eta$ and 3η using antiprotons in flight. The exper-

iment was performed with the Crystal Barrel detector at LEAR. Earlier data from this experiment on $\bar{p}p$ annihilation at rest have revealed several $J^P = 0^+$ resonances [1–3]. The present study is aimed at higher masses. In particular, it is important to locate $I = 1$ $\bar{q}q$ radial excitations, in order to set a mass scale with which $I = 0$ resonances can be compared. This scale will provide clues as to which $I = 0$ resonances are likely to be $\bar{q}q$ states and which may be candidates for glueballs.

The $\pi^0\eta\eta$ data we report here were taken at a beam momentum of 1940 MeV/c, corresponding to a center of mass energy of 2409 MeV. They reveal evidence for an

^a Now at Cornell University, Ithaca, USA

^b Now at University of Freiburg, Freiburg, Germany

^c University of Ljubljana, Ljubljana, Slovenia

^d University of Silesia, Katowice, Poland

^e Now at Andersen Consulting, Frankfurt, Germany

^f This work is part of the PhD. thesis of J. Lüdemann

^g This work is part of the PhD. thesis of H. Stöck

^h Now at University of Bonn, Bonn, Germany

$I = 1$, $J^P = 2^+$ resonance at 1660 MeV/c² decaying to $\pi^0 \eta$. This resonance is a natural candidate for the radial excitation of $a_2(1320)$. There has been tentative evidence for a resonance at (1624 ± 50) MeV/c² from our earlier $2\pi^0 \eta$ data at rest [3]. In those data, the available mass range was limited to 1740 MeV/c²; the present data expand the $\pi^0 \eta$ mass range to 1861 MeV/c².

In the $\eta\eta$ channel, the available mass range extends to 2274 MeV/c². Near the top of this range, we observe a strikingly strong $\eta\eta$ signal. It is centered at 2140 - 2160 MeV/c², according to whether it is fitted with $J^P = 0^+$, 2^+ or 4^+ .

The layout of this paper is as follows. Section 2 describes the features of the experiment relevant to the 6γ final state and section 3 introduces the procedures for selecting events. Section 4 describes the amplitude analysis used to fit the data. In Section 5, the evidence for the $\pi^0 \eta$ resonance at 1660 MeV is discussed. This resonance occurs in a different part of the Dalitz plot than the $\eta\eta$ peak at 2140 - 2160 MeV/c², so that the two phenomena are almost completely decoupled in the analysis. Section 6 discusses the latter phenomenon assuming that it is due to a single resonance. Section 7 describes the final fit and section 8 gives concluding remarks.

2 Experimental set-up

A full technical description of the detector has been given earlier [4]. It is a 4π solenoidal detector with good detection of both γ and charged particles. For present purposes, the γ detection is crucial. A barrel of 1380 CsI crystals, each of 16 radiation lengths, covers 98% of the laboratory solid angle around a liquid hydrogen target, 4.4 cm long. These crystals provide efficient γ detection with good energy resolution, $\sigma(E)/E = 0.025/[E(\text{GeV})]^{1/4}$, and good angular resolution, ± 20 mrad in both polar and azimuthal angles. For data using antiprotons of 1.94 GeV/c, the Lorentz boost increases the geometrical acceptance for photons in the backward direction and decreases it in the forward direction; the overall solid angle covered in the center of mass is 95% of 4π .

Cylindrically surrounding the target are two multi-wire proportional chambers, which are used on-line to veto events producing charged particles. They cover 98% of the solid angle in the laboratory frame. A veto counter downstream eliminates non-interacting particles and elastic scattering in the diffraction region. Outside the two multi-wire chambers is a cylindrical jet drift chamber which serves as the central detector for measuring charged tracks. In the present work, it is used only for extra veto against charged particles.

3 Event reconstruction and selection

During the years 1992 and 1994, 10.5 million events from $\bar{p}p$ annihilation were recorded with the Crystal Barrel detector at an incident \bar{p} momentum of 1.94 GeV/c, the

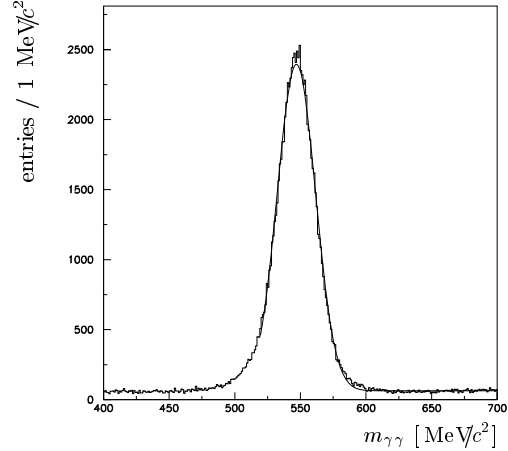


Fig. 1. The $\gamma\gamma$ invariant mass spectrum near the η peak from events fulfilling the hypothesis $\bar{p}p \rightarrow \pi^0 \pi^0 \gamma\gamma$.

maximum available at LEAR. The trigger demanded an interacting antiproton and a neutral final state. This trigger required signals from two entrance counters in coincidence and no signal from the veto counter downstream of the target. It also demanded the absence of hits in the proportional wire chambers and in two (at times three) of the innermost layers of the jet drift chamber. In addition, an on-line threshold of 2 GeV was set on the total energy deposited in the electromagnetic calorimeter [5]. This requirement enriched the data in neutral events in which the full energy of the interaction was detected.

The off-line reconstruction was similar to that for data at rest [1–3]. Cuts were applied to reject any residual events with charged tracks in the jet drift chamber, and exactly six photons in the calorimeter were demanded. Only crystals with a deposited energy of at least 1 MeV were taken into account. For reconstruction of a photon, a minimum energy of 20 MeV was required in a group of adjacent crystals. There were two differences in the data treatment compared to the analysis at rest. (1) Events with conversions centered in the crystals next to the beam-pipe were rejected for data at rest. In the present analysis, conversions in crystals immediately adjoining the downstream hole of the CsI-detector were kept in order to minimize the number of events lost because of the Lorentz boost. The subsequent kinematic fits eliminated events where any significant energy was lost from these crystals into the beam-pipe. (2) Because of the Lorentz boost, roughly 40% of π^0 in the forward hemisphere gave rise to two photons whose showers overlapped partially. These events were successfully reconstructed when two separate peaks could be identified in separate crystals within one cluster. It turned out that the problem of two γ hits giving rise to a merged signal in the CsI-detector was not significant for this data set.

In the analysis, only π^0 and η decaying into two photons were considered. The final states $3\pi^0$, $2\pi^0 \eta$, $\pi^0 \eta \eta$ and

Table 1. Efficiencies for reconstruction of $\pi^0\eta\eta$ events and suppression of background. The numbers give the feed through fractions of Monte Carlo events which survive all cuts and are finally identified as $\pi^0\eta\eta$. Here it is assumed, that all channels have the same branching ratio.

final state	selected fraction
$3\pi^0$	3×10^{-5}
$2\pi^0\eta$	4×10^{-5}
$\pi^0\eta\eta$	23.5%
3η	1×10^{-3}
$\pi^0\omega$	3×10^{-5}
$\eta\omega$	6×10^{-4}
$\omega\omega$	3×10^{-4}
$2\pi^0\omega$	6×10^{-5}
$\pi^0\eta\omega$	2×10^{-3}
$4\pi^0$	$< 1 \times 10^{-5}$

3η were reconstructed from six measured photon hits in the calorimeter. The following hypotheses were tested in the following sequence [6]

- (1) $\bar{p}p \rightarrow 6\gamma$
- (2) $\bar{p}p \rightarrow \pi^0 \pi^0 \gamma\gamma$
- (3) $\bar{p}p \rightarrow \pi^0 \pi^0 \pi^0$
- (4) $\bar{p}p \rightarrow \pi^0 \pi^0 \eta$
- (5) $\bar{p}p \rightarrow \pi^0 \eta\eta$
- (6) $\bar{p}p \rightarrow \eta\eta\eta$.

The fit allowed an unknown position along the beam axis for the reaction vertex in the liquid hydrogen target. From the $\gamma\gamma$ invariant mass spectrum (fig.1) of events fulfilling hypothesis (2) with a confidence level greater than 10% and hypothesis (3) with less than 1%, the resolution near the η can be estimated by fitting a gaussian to the spectrum. This gives a resolution of $\sigma = 14.6$ MeV/c² for the reconstructed $\gamma\gamma$ invariant mass around 550 MeV/c².

The final state $\pi^0\eta\eta$ was selected by requiring a confidence level greater than 10% for hypothesis (5). Veto cuts were applied against the prolific reactions (3) and (4) rejecting events with a confidence level larger than 10^{-5} . A confidence level cut at 10% was adequate to reject 3η -events. The selection resulted in 5831 $\pi^0\eta\eta$ -events. Additionally, $\sim 197\,000$ $3\pi^0$ -, $\sim 95\,000$ $2\pi^0\eta$ - and 473 3η -events were reconstructed.

The efficiency for reconstruction and selection of $\pi^0\eta\eta$ -events was estimated using a full Monte Carlo (MC) simulation of the detector based on the GEANT [7] program. Feed-through from background channels was estimated in the same way. Approximately 100 000 events were generated for each of the reactions $\bar{p}p \rightarrow 3\pi^0$, $\rightarrow 2\pi^0\eta$, $\rightarrow \pi^0\eta\eta$, $\rightarrow 3\eta$, $\rightarrow \omega\omega$, $\rightarrow 2\pi^0\omega$ and $\rightarrow \pi^0\eta\omega$ ($\omega \rightarrow \pi^0\gamma$) and reconstructed as described above. Furthermore, 50 000 $4\pi^0$ -events and 30 000 $\pi^0\omega$ - and $\eta\omega$ -events were investigated. Table 1 shows the fraction of events which were selected as $\pi^0\eta\eta$ -events after passing the reconstruction chain. From our data (see above), the known reconstruction efficiencies and the 2γ -branching ratios of π^0 and η [8], the relative branching ratios of $2\eta\pi^0$ -, $2\pi^0\eta$ - and $3\pi^0$ -channels can be determined: $\text{BR}(2\eta\pi^0)/\text{BR}(3\pi^0)=0.21$;

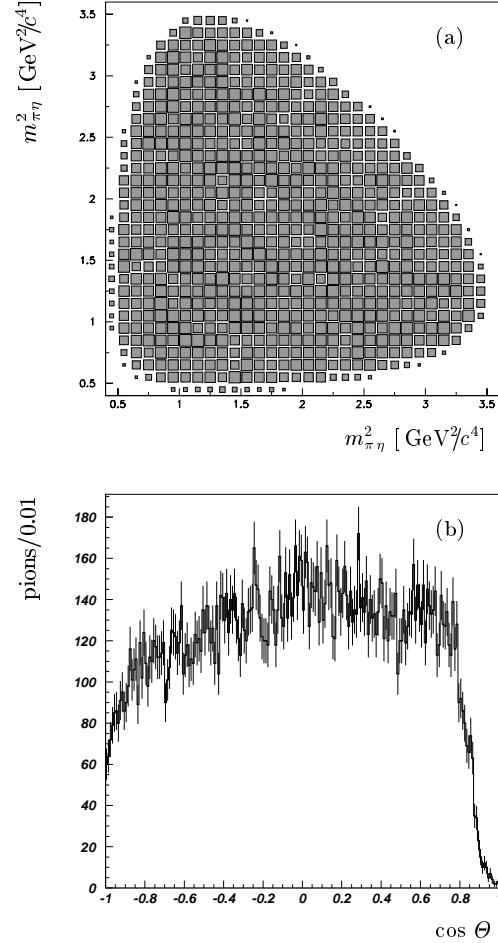


Fig. 2. The acceptance for the final state $\pi^0\eta\eta$. Figure (a) shows the Dalitz plot for Monte Carlo generated events. In figure (b) is shown the distribution of the cosine of the angle between the pion and the beam direction for simulated events in the $\bar{p}p$ center of mass.

$\text{BR}(2\eta\pi^0)/\text{BR}(2\pi^0\eta)=0.19$. Taking these numbers as typical for the channels under discussion (Table 1), it turns out, that the contamination from falsely interpreted background reactions is at most in the order of several percent. A Monte Carlo simulation showed, that it is uniformly distributed over the Dalitz plot.

23 539 MC-events have been used for the analysis. Fig. 2 (a) shows the acceptance of the apparatus for the MC-events assuming a phase space distribution for generated events. No structures due to acceptance variations are found in the Dalitz plot. Fig. 2 (b) shows the distribution of the cosine of the angle θ between the π^0 and the beam axis in the $\bar{p}p$ center of mass. The pion angular acceptance is almost uniform, but drops sharply for π^0 close to the beam pipe ($|\cos\theta| = 1$).

Figure 3 shows the data, i.e. the Dalitz plots and the spectra of invariant masses for the reaction $\bar{p}p \rightarrow \pi^0\eta\eta$. Ac-

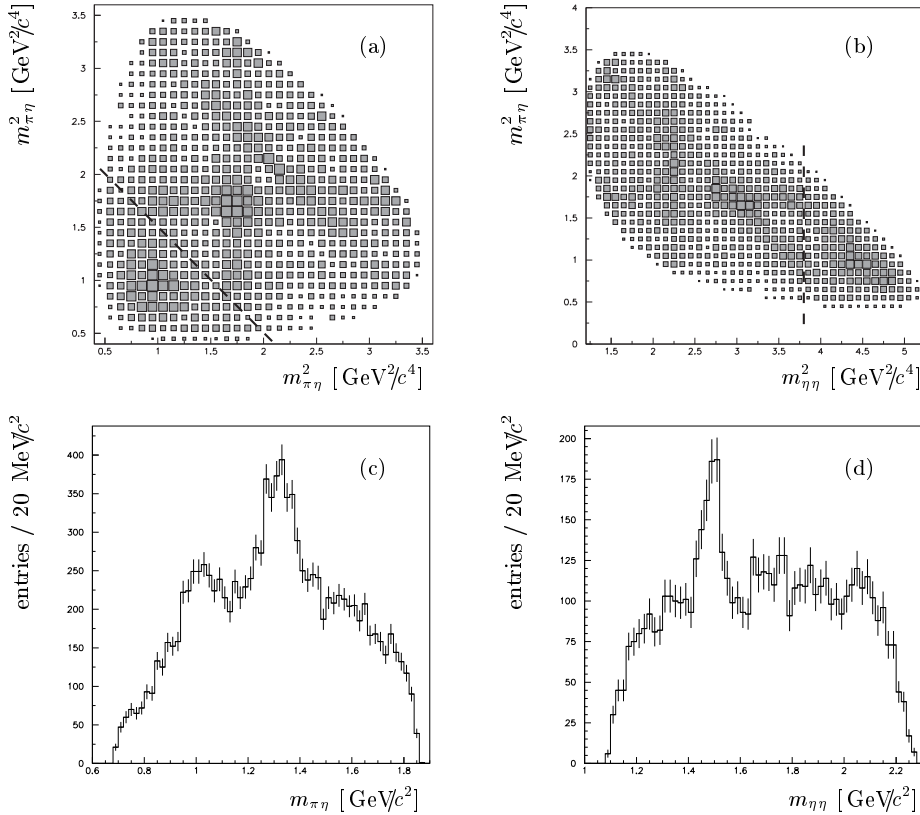


Fig. 3. Dalitz plots and invariant mass distributions for the reaction $\bar{p}p \rightarrow \pi^0 \eta \eta$ at 1.94 GeV/c. Plot (a) shows the symmetric Dalitz plot, (b) the asymmetric one. Spectrum (c) shows the spectrum of $\pi^0 \eta$ invariant masses (2 entries/event), (d) the $\eta \eta$ invariant masses (1 entry/event). The broken line shows the cut in $m_{\pi\eta}^2$ as described in section 5.

ceptance corrections are not included, but they were later applied during the fits of the data via Monte Carlo simulation. In Fig. 3 (a) vertical and horizontal bands from the $\pi^0 \eta$ resonances $a_0(980)$ and $a_2(1320)$ show up, and a diagonal band at an $\eta\eta$ invariant mass around 1500 MeV/c² is clearly visible. In addition, there is a structure at high $\eta\eta$ masses (~ 2150 MeV/c²) in the lower left corner of the Dalitz plot, partially hidden by the crossing of the $a_0(980)$ bands. We shall show that this strong enhancement at high $\eta\eta$ masses is not due to the $a_0(980)$ only, but requires at least one high mass resonance.

4 Formalism of the analysis

The analysis is based on the isobar model [9] and uses relativistic Breit-Wigner amplitudes to describe the resonances. Unfortunately, due to the many angular momentum states of the initial $\bar{p}p$ system contributing to the annihilation process in flight, a full analysis describing both production and decay of the resonances was not successful. Hence a simplified ansatz was worked out using only the decays of the intermediate states, thus averaging over

the production variables. This formalism was used for the first time in ref. [10].

The analysis integrates over the production dynamics of the initial state. In order to outline the formalism, let us take as example the process $\bar{p}p \rightarrow a_2(1320)\eta_2$, $a_2(1320) \rightarrow \eta_1 \pi^0$. The $a_2(1320)$ may be produced with spin components $\lambda = +2$ to -2 along the beam direction which is chosen as quantization axis. The cross sections for spin components λ and $-\lambda$ are identical. The amplitudes for the components $\lambda = 2, 1$ and 0 have different complex coupling constants, and the decay of the $a_2(1320)$ from each component is described by spherical harmonics $Y_2^\lambda(\alpha_1, \beta_1)$. The angles α_1 and β_1 are the polar and azimuthal decay angles of η_1 with respect to the beam direction, after a Lorentz transformation to the rest frame of the $a_2(1320)$; full details of this transformation are explained in [10], and follow the standard treatment of Bourrely, Leader and Soffer [11]. E.g., the $a_2(1320)$ decay to $\pi^0 \eta_1$ is thus described by a Breit-Wigner amplitude:

$$A_{a_2(1320)}^\lambda(m) = a_{a_2(1320),\lambda} \Delta(m) Y_2^\lambda(\alpha_1, \beta_1) e^{i\delta_{a_2(1320)}} \quad (1)$$

with $a_{a_2(1320),\lambda}$ and $\delta_{a_2(1320)}$ being the magnitude and the phase of the complex coupling constant. The λ -dependence

$$\begin{aligned}
 I(\tau) = & a_{f_0(1500)}^2 |\Delta_{f_0(1500)}(m')|^2 \\
 & + a_{f_0(980)}^2 |\Delta_{f_0(980)}(m')|^2 \\
 & + \sum_{\lambda=0,1,2} a_{f_2(1270),\lambda}^2 |\Delta_{f_2(1270)}(m') Y_2^\lambda(\alpha, \beta)|^2 \\
 & + \sum_{k=1,2} a_{a_0(980)}^2 |\Delta_{a_0(980)}(m_k)|^2 \\
 & + \sum_{\lambda=0,1,2} a_{a_2(1320),\lambda}^2 \sum_{k=1,2} |\Delta_{a_2(1320)}(m_k) Y_2^\lambda(\alpha_k, \beta_k)|^2 \\
 & + Re \sum_{k,k'=1,2} a_{a_0(980)} a_{a_2(1320),0} c_{a_0(980)a_2(1320),0} e^{i\delta_{a_0(980)a_2(1320)}} \Delta_{a_0(980)}(m_k) \Delta_{a_2(1320)}^*(m_{k'}) Y_2^0(\alpha_{k'}, \beta_{k'}) \\
 & + Re \sum_{k=1,2} a_{a_0(980)} a_{f_0(1500),0} c_{a_0(980)f_0(1500),0} e^{i\delta_{a_0(980)f_0(1500)}} \Delta_{a_0(980)}(m_k) \Delta_{f_0(1500)}^*(m') \\
 & + Re \sum_{k=1,2} a_{f_0(1500)} a_{a_2(1320),0} c_{f_0(1500)a_2(1320),0} e^{i\delta_{f_0(1500)a_2(1320)}} \Delta_{f_0(1500)}(m') \Delta_{a_2(1320)}^*(m_k) Y_2^0(\alpha_k, \beta_k) \\
 & + Re \sum_{k=1,2} a_{a_0(980)} a_{f_2(1270),0} c_{a_0(980)f_2(1270),0} e^{i\delta_{a_0(980)f_2(1270)}} \Delta_{a_0(980)}(m_k) \Delta_{f_2(1270)}^*(m') Y_2^0(\alpha_k, \beta_k) \\
 & + Re \sum_{\lambda=0,1,2} \sum_{k=1,2} a_{a_2(1320),\lambda} a_{f_2(1270),\lambda} c_{a_2(1320)f_2(1270),\lambda} e^{i\delta_{a_2(1320)f_2(1270)}} \Delta_{a_2(1320)}(m_k) \Delta_{f_2(1270)}^*(m') \\
 & \quad Y_2^\lambda(\alpha_k, \beta_k) Y_2^{\lambda*}(\alpha, \beta) \\
 & + Re a_{a_0(980)}^2 c_{a_0(980)a_0(980)} \Delta_{a_0(980)}(m_1) \Delta_{a_0(980)}^*(m_2) \\
 & + Re \sum_{\lambda=0,1,2} a_{a_2(1320),\lambda}^2 c_{a_2(1320)a_2(1320),\lambda} \Delta_{a_2(1320)}(m_1) \Delta_{a_2(1320)}^*(m_2) Y_2^\lambda(\alpha_1, \beta_1) Y_2^{\lambda*}(\alpha_2, \beta_2) \tag{2}
 \end{aligned}$$

of δ is suppressed in order to reduce the number of parameters. m is the invariant $\pi^0 \eta$ -mass and

$$\Delta(m) = \frac{m_0 \Gamma_0 B_L(q, q_0)}{m^2 - m_0^2 - im_0 \Gamma(m)} \tag{3}$$

where

$$\Gamma(m) = \Gamma_0 \sum_i \gamma_i^2 \rho_i B_L^2(q_i, q_{i,0}) \tag{4}$$

(i = sum over all relevant decay channels). m_0, Γ_0 are the nominal mass and width of $a_2(1320)$, q is the $\pi^0 \eta$ -break-up momentum, $q_0 = q(m_0)$, B_L the angular momentum barrier function as defined in [12], $\rho_i = 2 \frac{q_i}{m}$ the phase space factor for channel i and γ_i the weight factor for decay mode i ($\sum_i \gamma_i^2 = 1$). For resonances with yet unknown branching ratios, like $a_2(1660)$ and $f_J(2140-2160)$,

$$\Delta(m) = \frac{m_0 \Gamma_0}{m^2 - m_0^2 - im_0 \Gamma_0} \tag{5}$$

was used.

$$\begin{aligned}
 I(m, m') = & \sum_{\lambda} (|A_{a_2(1320)}^\lambda(m)|^2 + |A_{f_0(1500)}^\lambda(m')|^2 \\
 & + c_\lambda Re[A_{a_2(1320)}^{\lambda*}(m) A_{f_0(1500)}^\lambda(m')]) \tag{6}
 \end{aligned}$$

with m and m' being the masses of the $\pi^0 \eta$ - and the $\eta \eta$ -pair, respectively. The coefficients c_λ in the interference term express the partial coherence and lie in the range +2 to -2. Likewise, at the crossing of two $a_2(1320)$ bands on the Dalitz plot, the interference between the two $a_2(1320)$ is only partially coherent, and requires coefficients c_λ .

The intensity for the final state is given by the sum of squares of amplitudes over all channels. There are no interferences between different spin components λ , because they have different azimuthal dependence which average to zero. A complication, however, is that one must allow for the fact that a resonance is not produced from a single initial partial wave, but from many. Each partial wave gives different Clebsch-Gordan coefficients and different angular dependences in the production process. We average over the production, so that interferences of e.g.

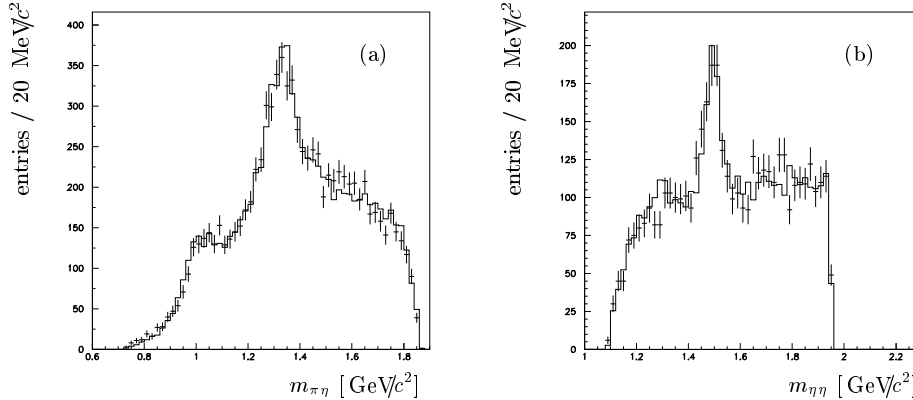


Fig. 4. Invariant mass spectra of the final state $\pi^0\eta\eta$ plotted as error bars, with the result of the first fit superimposed as a solid line. Fig. (a) shows the $\pi^0\eta$ invariant mass distribution, plot (b) the $\eta\eta$ invariant mass distribution.

$a_2(1320)$ with another resonance, say $f_0(1500)$, are not fully coherent, but only partially coherent. In this case, the intensity I is given by

As an example, we give in equation (2) explicitly the intensity for the hypothesis of the first fit (see later) assuming three isoscalar resonances $f_0(1500)$ (row 1), $f_0(980)$ (row 2) and $f_2(1270)$ (row 3), and two isovectors $a_0(980)$ (row 4) and $a_2(1320)$ (row 5). Interferences are also taken into account between $a_0(980)$ and $a_2(1320)$ (row 6), $a_0(980)$ and $f_0(1500)$ (row 7), $f_0(1500)$ and $a_2(1320)$ (row 8), $a_0(980)$ and $f_2(1270)$ (row 9) and $a_2(1320)$ and $f_2(1270)$ (row 10). In addition, the interferences of the crossing $a_0(980)$ bands (row 11) and the crossing $a_2(1320)$ bands (row 12) in the Dalitz plot are taken into account. The indices k and k' refer to the two different $\pi^0\eta$ combinations in the final state. (α, β) are the decay angles of $\eta\eta$, (α_k, β_k) the decay angles of the k -th $\pi^0\eta$ -pair. The argument τ stands for the phase space coordinates uniquely describing the event. The quantity δ_{ab} is a shorthand for the phase difference $\delta_a - \delta_b$.

The free parameters of the fit are the couplings $a_{particle,\lambda}$ (real numbers), the strengths of the interferences $c_{particles,\lambda}$ (real numbers) and the phases $\delta_{particle}$. The masses and widths of the resonances, which are implicitly contained in the dynamical functions Δ are varied by hand and are not automatically optimized by the fitting procedure. Thus, in this case, the fit contains 24 parameters. One magnitude can be set to one and one phase can be chosen as zero, so that 22 free adjustable parameters remain.

5 Evidence for a 2^+ resonance in $\pi^0\eta$

The fit of the amplitudes to the data was carried out using the log likelihood method. In a first step to fit the data we limited the Dalitz plot to an $\eta\eta$ mass-square $< 3.8 \text{ GeV}^2/c^4$ (see Fig. 3). The remaining 4493 data and 18 996 Monte Carlo events were fitted assuming the resonances and interferences listed in Table 2. There is no evidence for any other f_0 -states, like $f_0(1370)$ e.g. it is not possi-

Table 2. Resonances and interferences as ingredients for the first fit.

Resonance	mass [MeV]	width [MeV]
$a_0(980)$	990	140
$a_2(1320)$	1330	190
$f_0(980)$	980	70
$f_2(1270)$	1280	230
$f_0(1500)$	1490	50

Interferences
$a_0(980) \times a_2(1320)$
$a_0(980) \times f_0(1500)$
$a_0(980) \times f_2(1270)$
$a_0(980) \times a_0(980)$
$a_2(1320) \times f_2(1270)$
$a_2(1320) \times f_0(1500)$
$a_2(1320) \times a_2(1320)$

ble to describe the obviously narrow $f_0(1500)$ by interferences with other scalars. The masses and widths of the resonances were kept fixed to the values given in Table 2, which were the result of a mass and width scan [13]. The mass dependence of the resonances was described by eq. (2). In the summation (4) only channels relevant for the line shape were taken into account. This description turned out to be satisfying in view of the small statistical sample, which is not very sensitive against the line shape. The fit function contained 22 free parameters (a_λ , c_λ and δ).

The fit converged to a negative logarithmic likelihood NLL of -392. The zero of the scale of NLL is arbitrary. Only the differences between NLLs can be compared. We use the standard definition of log likelihood, such that a change of 0.5 corresponds statistically to one standard deviation. From our general experience in fitting other data, a change in log likelihood of 20 for the addition of one amplitude is strongly suggestive, and a change of 40 may be considered definitive with the statistics of the present

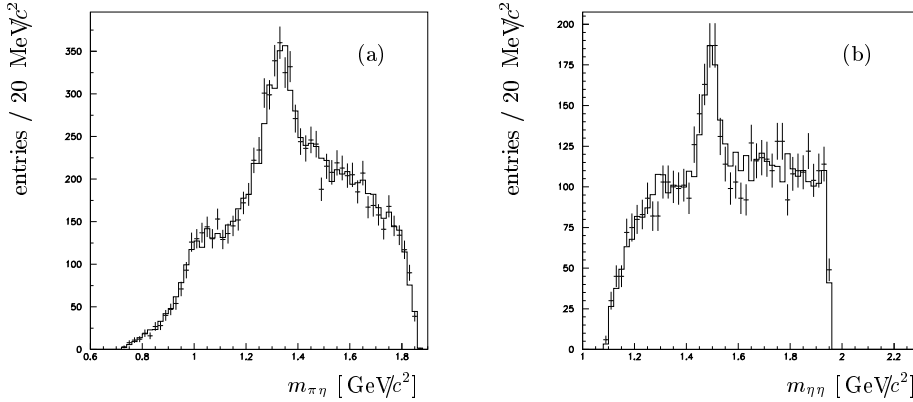


Fig. 5. Invariant mass spectra of the extended fit (first fit plus an a_2 around 1650 MeV/c²).

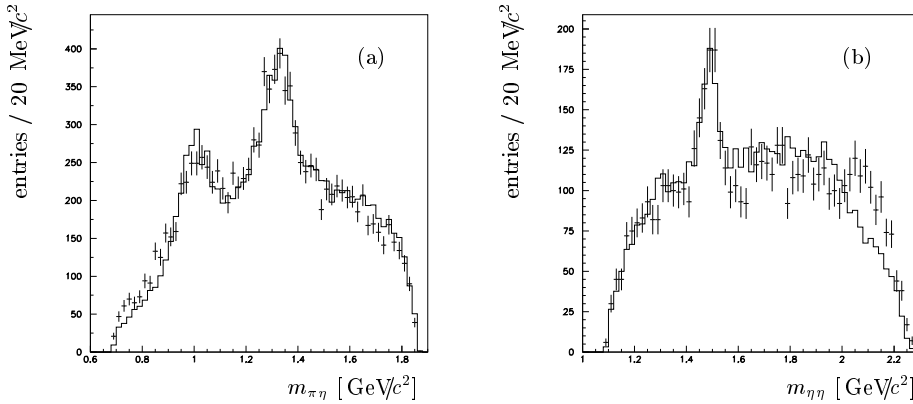


Fig. 6. Invariant mass spectra of the extended fit on the full Dalitz plot.

data. These numbers provide a rough guideline for the significance of new components in the fit.

The mass projections of the first fit are shown in figure 4. The fit is satisfying except for the $\pi^0\eta$ -mass range between 1.4 and 1.8 GeV/c², where systematic over- and undershoots are visible. Therefore we have tried adding an a_0 (1450), a ρ (1400) and an f_0 (1300). None improves the fit in a significant way [13].

The fit improves significantly with the introduction of a new isovector resonance with J=2 and a mass around 1650 MeV/c² and a width of 300 MeV/c². Including its interferences with a_0 (980) and a_2 (1320) NLL decreased by 91 to -483, now fitting 33 parameters. The mass spectra of this extended fit are shown in figure 5. The existence of the new a_2 (1660)-state is only marginally visible in the Dalitz plot projections. The main evidence comes from the dramatic improvement in NLL. However, the $\pi\eta$ -mass region between 1500 and 1700 MeV/c² is better described when taking into account the new state (Fig. 4a/5a). Such a behaviour is not uncommon for a broad resonance in the presence of many interfering states. In turn we tested also an f_J (1700) with J = 0 and 2, and an f_2 (1525). Both resonances were rejected by the fit.

Table 3. Results of fits using an f_J (2100) with different spins as compared to the extended fit.

Spin	NLL	Δ NLL	$\Delta\#$ parameter	optimized mass/width
0	-560	135	4	2130 / 180
2	-628	203	8	2140 / 310
4	-671	246	10	2150 / 230

In the next step we tried to fit the ingredients of the extended fit on the full Dalitz plot. After optimization the fit ended up with a NLL of -425. Note, that this value cannot be compared to the NLL of the extended fit on the reduced Dalitz plot due to the different data sample. The fit result is displayed in fig. 6. It is obvious that there is a large discrepancy at the a_0 (980) crossing region which corresponds to the $\eta\eta$ mass region around 2.1 GeV. This region cannot be explained by a_0 (980) crossing alone, even if one uses a Flatté-parametrization for the a_0 (980), and suggests the presence of at least one $\eta\eta$ resonance around 2100 MeV/c².

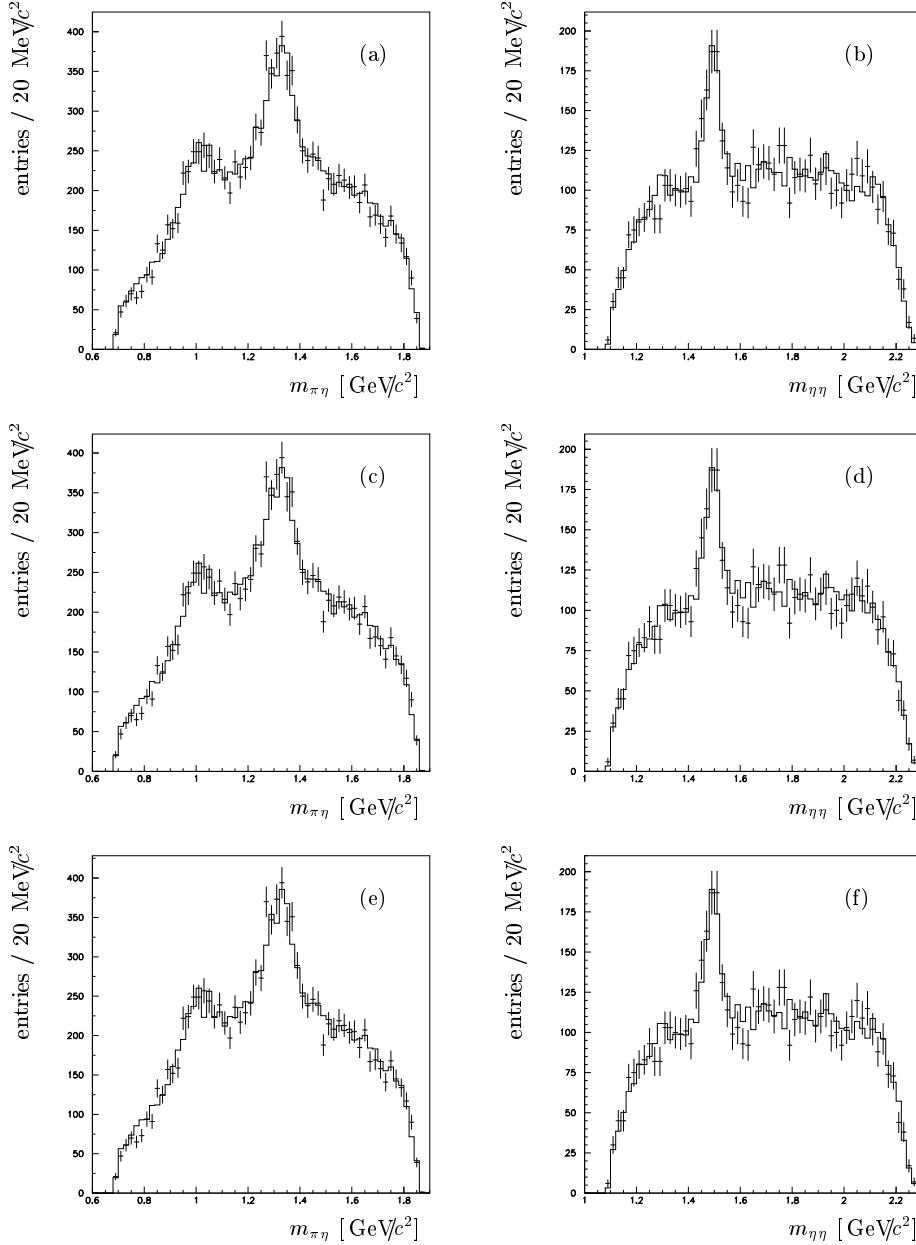


Fig. 7. Invariant mass spectra of the extended fit adding a $f_J(2100)$. (a) and (b) show the $\pi^0\eta$ and $\eta\eta$ mass projections for spin 0. Spectra (c) and (d) present a fit with spin 2 and spectra (e) and (f) a fit with spin 4.

6 Evidence for an $\eta\eta$ resonance around 2.1 GeV/c²

To describe the $\eta\eta$ mass region around 2.1 GeV/c² we introduced an $f_J(2100)$ with $M = 2150$ MeV/c² and $\Gamma = 300$ MeV/c². In addition we allowed interferences with $a_0(980)$ and $a_2(1320)$. The resulting NLL depends on the spin J of the resonance, but shows a large improvement for each spin (Tab. 3). Although every spin gives a significant change in NLL we cannot definitely distinguish between

them. This is also visible in the invariant $\eta\eta$ mass projections shown in figure 7. The visible change in the projections between different spin assumptions is marginal and demonstrates only the necessity for the introduction of a new resonance. For simplicity we consider mainly $J=2$ in subsequent discussions, since the spin does not affect the final conclusions.

To perform a cross-check we fitted the upper $\eta\eta$ mass part of the Dalitz plot separately. Only data with $m^2(\eta\eta) \geq 3.8$ GeV²/c⁴ were considered. The 1.338 data and 4.543

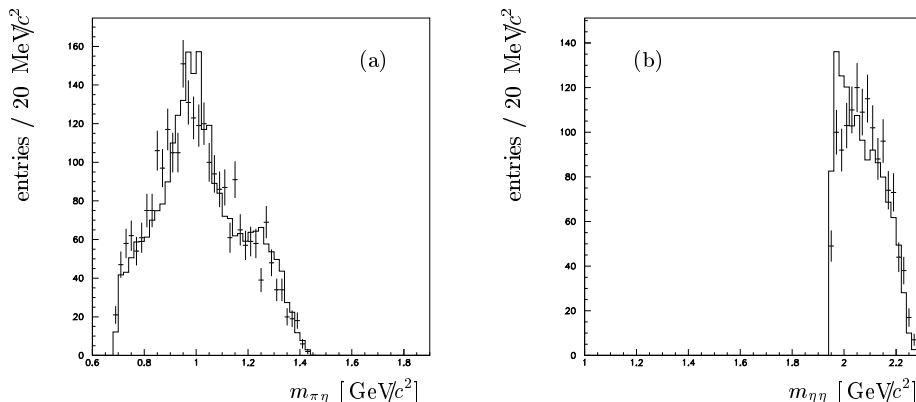


Fig. 8. Invariant mass spectra of the high $\eta\eta$ mass region. The fit was performed without an $f_2(2100)$.

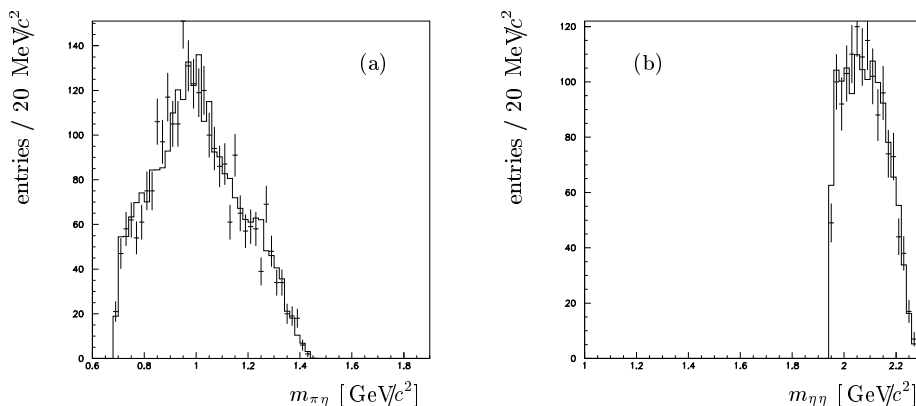


Fig. 9. Invariant mass spectra of the high $\eta\eta$ mass region fit including an $f_2(2100)$.

Monte Carlo events were fitted assuming an $a_0(980)$, an $a_2(1320)$ and an $f_2(2100)$. First a fit using the $a_0(980)$ and the $a_2(1320)$ was performed. We took only the interference $a_0(980) \times a_2(1320)$ and the $a_0(980)$ self-interference into account, because the $a_2(1320)$ crossing region is outside the considered part of the Dalitz plot. The fit resulted in a NLL of -23 using 6 parameters. The invariant mass projections are shown in fig. 8. Clearly a discrepancy in the $\eta\eta$ invariant mass projection is visible. After including an $f_2(2100)$ and its interferences with the isovectors the NLL decreased to -107 (14 parameters). Figure 9 again demonstrates the necessity of an $f_J(2100)$ in this mass region.

7 Final fit

To describe the data in a proper way a final fit was performed. The ingredients were basically the same as for the extended fit, but the masses and widths were optimized after detailed scans. It requires the following resonances: $a_0(980)$, $a_2(1320)$, $a_2(1660)$, $f_0(980)$, $f_2(1270)$, $f_0(1500)$, $f_J(2100)$. Also interferences between some of them are necessary (see Table 4). We assumed $J=2$ for $f_J(2100)$. With these ingredients the final fit ended up with a NLL

of -629 using 41 parameters. The Dalitz plots and invariant mass projections are shown in figure 10. To visualize the quality of the fit, the χ^2/bin is plotted for the cases where the fit is greater than the data and vice versa (fig. 11). No systematic structures are visible. The overall value of $\chi^2/\text{d.o.f.}$ is 1.31. The $\eta\eta$ -mass projection between 1.6 and 2.0 GeV/c² shows fluctuations, which are not describable by the fit. In order to improve on the fit, a further $\eta\eta$ -resonance was introduced, the mass of which was allowed to vary between 1.6 and 2.0 GeV/c². No conclusive results were obtained.

The masses and widths of all resonances included in the final fit are listed in Table 5 (Col. 2 and 3). The errors correspond to the values, which produce a change of one in the NLL-values. In addition, we allowed for systematic uncertainties for masses (20 MeV/c²) and widths (50 MeV/c²). They were estimated from fits using different line shapes. The masses of the well known resonances agree within the errors with the PDG [8] values. In the widths discrepancies exist which may be due to the strong interference effects in the data. A fit with the nominal masses and widths of PDG worsened the overall NLL by 33, but produced no hints as to additional resonances that could

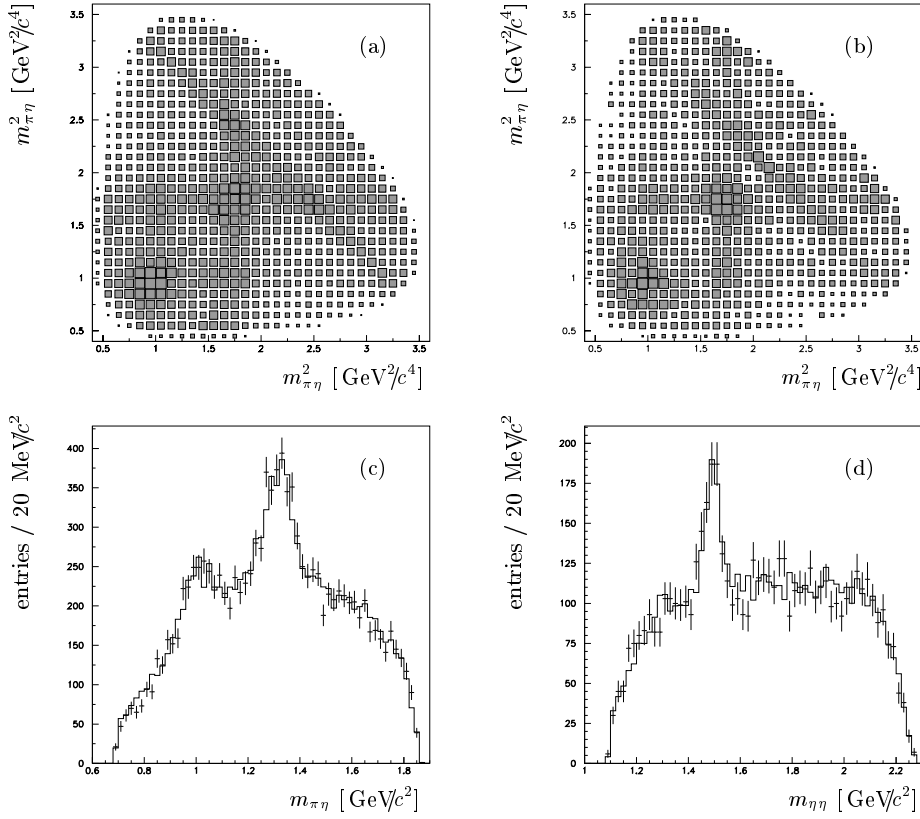


Fig. 10. Dalitz plots and invariant mass distributions of the final fit. (a) corresponds to the best fit, (b) represents the data Dalitz plot. (c) and (d) give the mass projections with the best fit results.

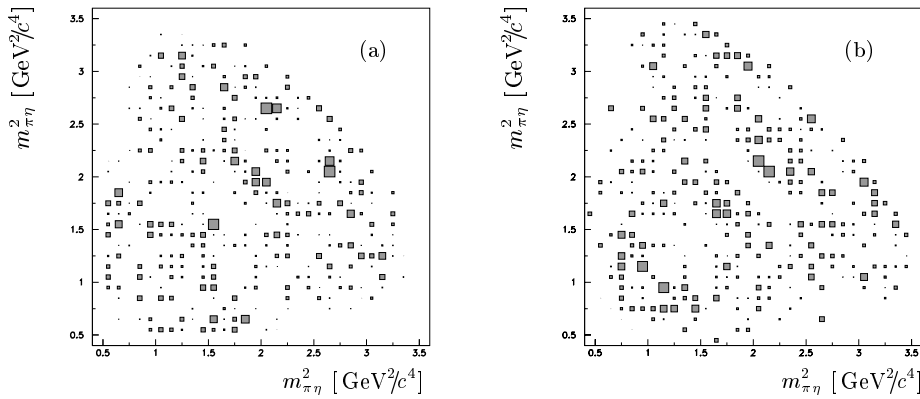


Fig. 11. $\Delta\chi^2$ distribution of the final fit. In plot (a) $\Delta\chi^2$ is presented for the case fit > data and in plot (b) for the case fit < data. The largest square represents a deviation of 3σ or more.

significantly contribute to the total intensity. Column 4 of Table 5 gives the percentage contributions of the states to the total intensity in the Dalitz plot. Note that only the squares of the amplitudes were taken into account. This procedure gives only a very rough estimate, because the patterns in the Dalitz plot are dominated by interference effects. These errors of the relative contributions are at

least 25%. The errors correspond to changes of the masses and widths of the resonances within their errors, always taking the extreme mass/width-combination.

Table 4. List of possible interferences between the states of the final fit. Only the interferences marked with \times are taken into account. The reason for leaving out others are: (a) no overlap, (b) no contribution (tested), (c) no existence.

	$f_0(980)$	$f_2(1270)$	$f_0(1500)$	$f_2(2100)$	$a_0(980)$	$a_2(1320)$	$a_2(1660)$
$f_0(980)$	c						
$f_2(1270)$	b	c					
$f_0(1500)$	a	b	c				
$f_2(2100)$	a	a	a	c			
$a_0(980)$	a	\times	\times	\times	\times		
$a_2(1320)$	b	\times	\times	\times	\times	\times	
$a_2(1660)$	b	b	b	a	\times	\times	\times

Table 5. Masses and widths of the resonances resulting from the final fit (Col. 1 and 2). Column 3 gives the percentage contribution of the resonance to the total intensity in the Daltiz plot.

Resonance	mass (error) [MeV/c ²]	width (error) [MeV/c ²]	contribution [%]
$a_0(980)$	990 (15)	140 (40)	11
$a_2(1320)$	1325 (20)	180 (30)	41
$a_2(1660)$	1660 (40)	280 (70)	18
$f_0(980)$	980 (50)	70 (30)	5
$f_2(1270)$	1280 (40)	200 (50)	4
$f_0(1500)$	1490 (10)	50 (20)	4
$f_J(2100)$ J = 2	2140 (30)	310 (50)	17

8 Summary

We report the observation of an isovector resonance with quantum numbers $J^{PC} = 2^{++}$ in its decay into $\pi^0\eta$. It has a mass of (1660 ± 40) MeV/c² and a width of (280 ± 70) MeV/c². Furthermore at least one $f_J(2100)$ I=0-state is needed to describe the high $\eta\eta$ mass region. The fit optimized the mass to (2140 ± 30) MeV/c² and the width to (310 ± 50) MeV/c² for J = 2. In our analysis, the spin of this resonance could not be determined unambiguously from the data.

We would like to thank the technical staff of the LEAR machine group and of all the participating institutions for their invaluable contributions to the success of the experiment. We acknowledge financial support from the German Bundesministerium für Bildung und Wissenschaft, the Schweizerischer Nationalfonds, the British Particle Physics and Astronomy Research Council, the U.S. Department of Energy and the National Science Research Fund Committee of Hungary (contract No. DE-FG03-87ER40323, DE-AC03-76SF00098, DE-FG02-87ER40315 and OTKA T023635). K.M. Crowe and F.-H. Heinsius acknowledge support from the A. von Humboldt Foundation, and N. Djaoshvili from the DAAD.

References

1. C. Amsler et al., Phys. Lett. **B355** (1995) 425.
2. V.V. Anisovich et al., Phys. Lett. **B323** (1994) 233.
3. C. Amsler et al., Phys. Lett. **B333** (1994) 277.
4. E. Aker et al., Nucl.Instr.Meth. **A321** (1992) 69.
5. C.A. Baker et al., Nucl.Instr.Meth. **A394** (1997) 180.
6. J. Lüdemann, *Beobachtung von Resonanzen in der Proton-Antiproton Annihilation im Fluge in drei pseudoskalare Mesonen*, PhD thesis, Ruhr-Universität Bochum, 1995.
7. R. Brun et al., *GEANT 3 User's Guide*, CERN DD/EE/84-1, rev. 1987.
8. Particle Data Group, Phys. Rev. **D54** (1996) 1.
9. J. Pisut and M. Roos, Nucl.Phys. **B6** (1968) 325.
10. B. Adomeit et al., Zeit. f. Phys. **C71** (1996) 227.
11. C. Bourrely, E. Leader and J. Soffer, Phys. Rep. **59** (1980) 95.
12. F. von Hippel, C. Quigg, Phys. Rev. D **5** (1972) 624.
13. H. Stöck, *Analyse von Dreiteilchen Endzuständen in der Proton-Antiproton Annihilation*, PhD thesis, Ruhr-Universität Bochum, 1998.